Hierarchical Clustering Identifies Hub Nodes in a Model of Resting-State Brain Activity

Mark Wildie and Murray Shanahan
Department of Computing
Imperial College London, England
Email: {mark.wild05,m.shanahan}@imperial.ac.uk

***Abstract*—A novel clustering algorithm is presented for analyzing the temporal dynamics of synchronization in networks of coupled oscillators and applied to a model of resting-state brain activity. Connectivity in the model is based on a human-brain structural connectivity matrix derived from diffusion tensor imaging tractography. We find a strong correspondence between areas of high synchronization and highly connected "hub" nodes, anatomical regions forming the structural core of the network linking all areas of the brain. Such models have the potential to increase our understanding of the constraints placed on brain function by underlying anatomical structure.**

I. Introduction

The application of graph theory to the analysis of neural structure has led to a greater understanding of the organization of the human brain [1]. Continued advances in non-invasive structural imaging and tractography allow the connectivity of the brain to mapped in ever greater detail. By viewing the resulting set of white matter tracts between anatomical regions as a network of nodes in a connected graph, the human brain has been shown [2] to exhibit the small-world property [3] prevalent in natural systems. Dense local connectivity coupled with a small number of long-range connections results in an energy and informationally efficient architecture combining local functional specialization and global integration.

Applying graph theoretic measures of degree and centrality further identifies some nodes within this small-world architecture as highly connected "hub" nodes. These form an integrated core network linking all other major neural areas [4]. The spatial and topological centrality of anatomical regions forming the core network is indicative of a role in maintaining efficient global communication throughout the brain [5].

Similar analysis has been performed on functional connectivity matrices, derived from time-series data recorded through modes of functional imaging such fMRI, MEG or EEG. Connections between brain regions are typically based on measures of correlation, coherence or mutual information. Small-world properties have been observed in the topology of both spontaneous resting-state [6] and task-related networks [7]. Modular structure and central hub regions have also been identified in resting-state functional networks [8], [9].

Several recent studies have examined the relationship between structural and functional connectivity [10]. It is commonly assumed that functional activity reflects underlying anatomical structure, that brain regions connected by a large number of cortical projections are likely to be functionally related. At a higher level it is suggested that the slow-changing anatomical structure of the brain provides a framework that constrains the state space of fast-changing functional activity [11]. The relationship between the two is complex however, and the extent to which the dynamical properties of the brain are constrained by structure remains an open question [12]. A general positive correlation has been found between the degree of structural connectivity and resting-state functional activity [13], [14]. Several studies have also demonstrated functional relationships between brain regions with few or no direct cortical connections [10].

This paper presents a method of analyzing the temporal dynamics of synchronization within networks of coupled oscillators. We aim to both identify nodes in the network forming synchronous clusters of activity and track changes in cluster membership over time. There is significant evidence

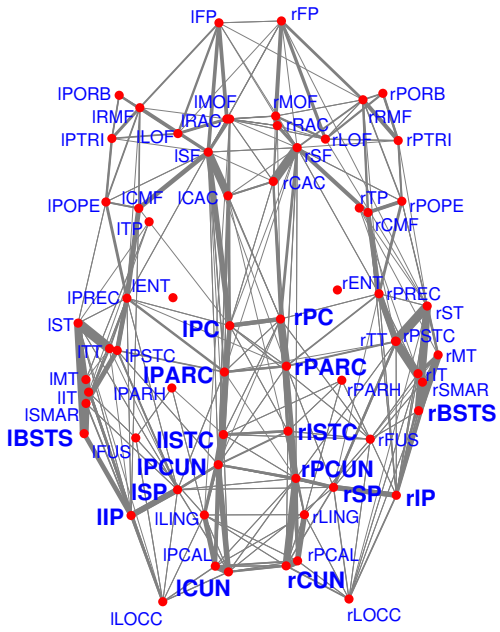

Fig. 1: Spatial representation of a 66-region human brain structural connectivity matrix [4] with relative density of connections between regions indicated by line thickness. Regions forming the structural core of the network are shown in bold.

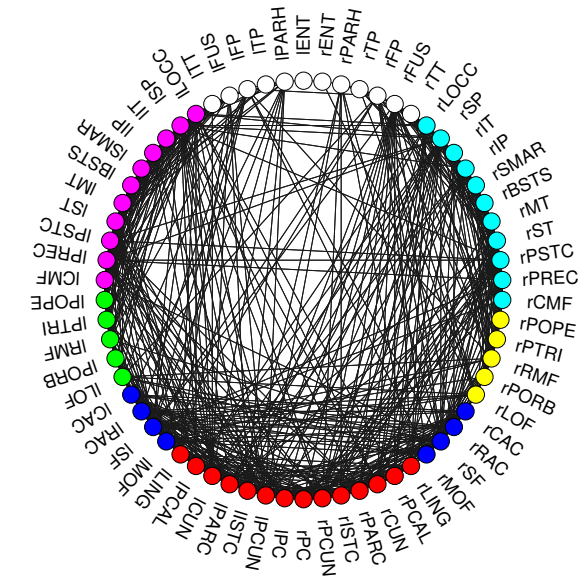

(a)

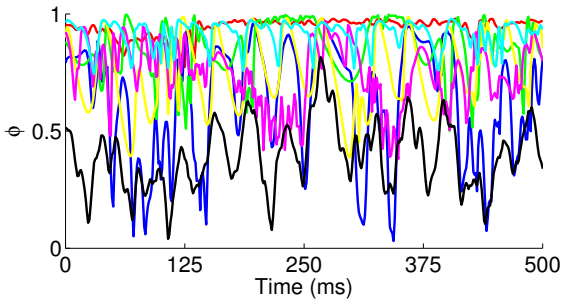

(b)

Fig. 2: a) Non-spatial representation of anatomical connectivity [4] ordered by hemisphere. Each labeled node corresponds to a single anatomical region, and each line to a connection between regions. b) Synchronization dynamics of a model of brain activity [15] based on the same connectivity matrix. Each anatomical region has been replaced by a single Kuramoto oscillator, and each structural connection by a weighted and delayed connection between oscillators. Each line represents the internal synchronization of a single cluster of oscillators (cluster membership identified by nodes of the same color). Global synchronization of the network is shown by a black line. The model displays metastable dynamics, where each cluster displays transient periods of synchronized and desynchronized activity.

for the functional importance of synchronous oscillation over multiple frequency bands in the human brain [16]. Changes in synchronization are proposed to underlie dynamic routing of information between neural areas [17]. As such, a method of identifying regions of synchronization within time-series neural data is a valuable tool for examining the occurrence of this type of potentially significant interaction. The described method is equally applicable to models of brain activity and data recorded from modes of functional imaging where oscillation is observed, such as EEG and fMRI. In this paper we apply the algorithm to a model of synchronization between connected brain regions, and show a close correspondence between synchronous dynamics and regions of modular structural connectivity within the model.

The rest of this paper is organized as follows. Section II provides an overview of the proposed algorithm and model of human brain activity. In Section III we present an analysis of activity within the model and comparison with structural properties of the network. Section IV concludes the paper and discusses future work.

Algorithm 1

Input:

- The matrix Φ, where for N nodes and t time steps $\Phi(i,j)$ is the phase θ_i of node i at time step j.
- The window length w_l.
- The window step size w_s.
- The synchrony threshold t.

Output:

- A set of clusters C_k each for window w_k of starting position $k \times w_s$ and end position $(k \times w_s) + w_l$, where each cluster $c \in C_k$ is a maximal non-overlapping subset of N with total synchrony $> t$.

Method:

Stage 1:

Partition Φ into $(s_l - w_l)/w_s$ windows of length w_l. We denote each window w_k, where $w_k(i)$ is the phase of node i from steps $k \times w_s$ to $(k \times w_s) + w_l$ for $i \in N$.

Stage 2:

for each w_k **do**

Stage 1:

Calculate the matrix D, where each entry $D(i,j)$ is the average pairwise synchrony ϕ_c between nodes i and j over w_k for $i,j \in N$ and $i \neq j$. Given $D(i,j) = D(j,i)$ we require $(n-1)!$ entries.

Stage 2:

while any two clusters remain where $D(i,j) > t$ **do**

1) Merge the two clusters with highest value $D(i,j)$.
2) Recalculate average ϕ_c over w_k for all remaining clusters and the newly merged cluster.
3) Update D.

end

end

II. Methods

A. Clustering Algorithm

A large number of clustering algorithms have been developed [18] and variations continue to be proposed. Our interest is in identifying subgroups of interacting nodes within larger networks that exhibit interesting dynamical properties. We aim to examine how those subgroups change over time for varying time scales. In the current model we consider changes in synchronization within a network of coupled oscillators, using the Kuramoto oscillator model [19] with time-delayed coupling. The phase θ_i of each oscillator is given by the equation

$$\frac{d\theta_i}{dt} = \omega + k \sum K_{i,j} \; sin\left(\theta_j(t-\tau) - \theta_i(t)\right) \qquad (1)$$

where ω is the natural frequency of the oscillator, $\theta_i\left(t\right)$ is the phase of oscillator i at time t, τ is a fixed time delay, k is a scaling factor and $K_{i,j}$ is the connection strength between oscillators i and j.

The instantaneous synchronization between any set of oscillators c at time t is given by

$$\phi_c\left(t\right) = \left| \left\langle e^{i\theta_k(t)} \right\rangle_{k \in c} \right| \qquad (2)$$

where $\theta_k\left(t\right)$ denotes the phase of oscillator k at time t and $\left\langle f \right\rangle_{k \in c}$ denotes the average of f over all k in c. The value ranges from $[0, 1]$, with 0 indicating complete desynchronization and 1 complete synchronization.

We take as input to the algorithm the combined time-series Φ, consisting of the phase of N oscillators at each of s_l time steps of resolution r. From Φ we generate windows of length w_l and step size w_s, where the kth window contains the phase of all oscillators from starting position $k \times w_s$ to position $(k \times w_s) + w_l$. Clustering is then performed individually for each of the $\left(s_l - w_l\right)/w_s$ windows. We take a hierarchical agglomerative approach to partitioning the network (Algorithm 1), where the closest two clusters are merged at every step of the algorithm until a synchronization threshold t. The distance between any two clusters is calculated as the combined instantaneous synchronization ϕ_c of all oscillators within both clusters averaged over the current window k. The algorithm completes when the combined average synchronization of any two clusters is below the threshold value.

B. Model

We use the model of human brain activity described in [15] for the generation of all results. A brief description of the connectivity matrix underlying the model follows, full details are given in [4]. The connectivity matrix covers 66 anatomical regions partitioned according to standard cortical anatomical landmarks. Connectivity between regions was obtained via

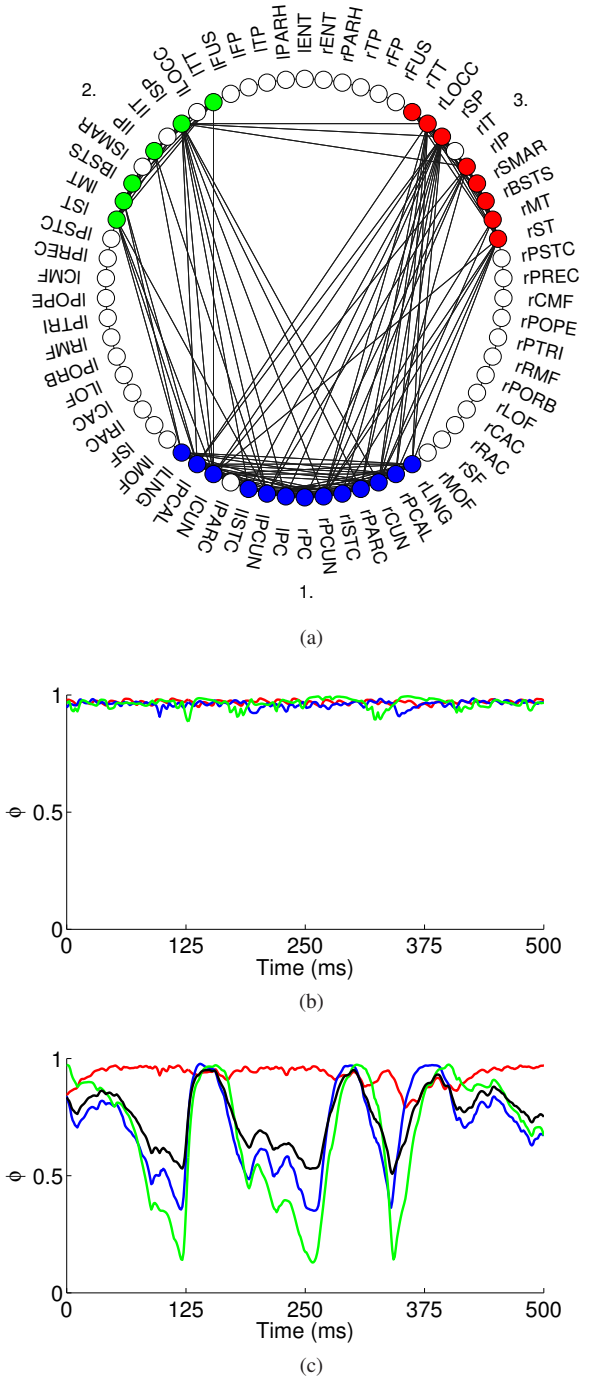

(a)

(b)

(c)

Fig. 3: Applying the algorithm over a long time window ($w_l = 4000$) identifies three clusters that maintain a constant high level of synchrony ($\phi_c > 0.95$). We label these 1, 2, and 3 and use the same labels to indicate these clusters in all following tables and figures. a) The anatomical connectivity within and between each cluster. b) The instantaneous synchronization over time of each cluster (cluster membership identified by nodes of the same color). c) The instantaneous synchronization of each combination of the three clusters (blue line = [1,2], red = [1,3], green = [2,3] and black = [1,2,3]).

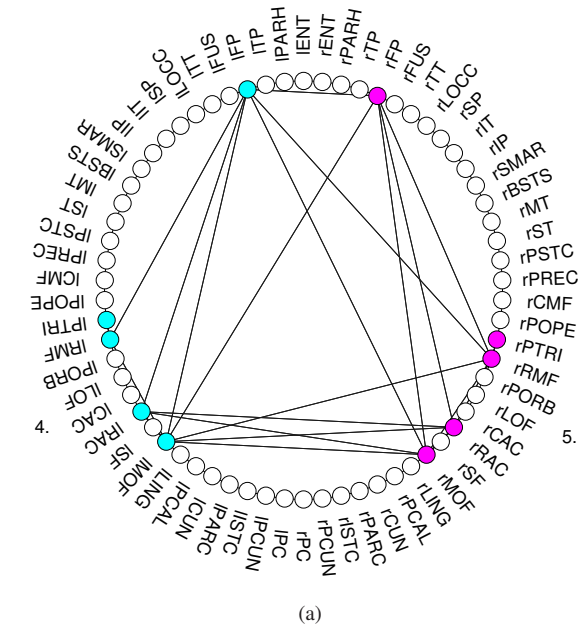

(a)

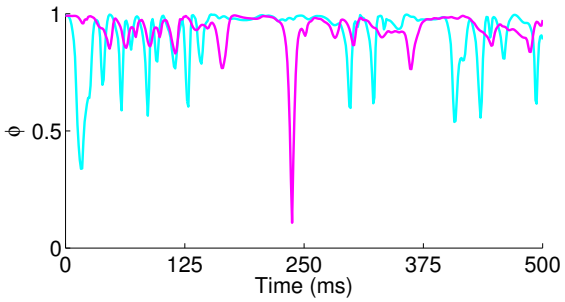

(b)

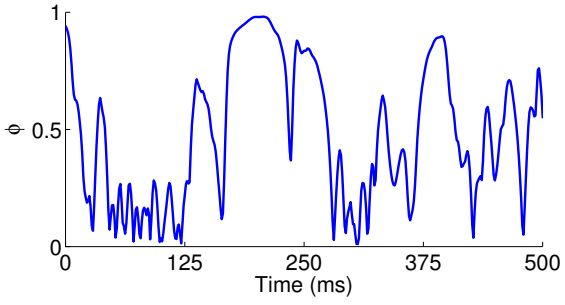

(c)

Fig. 4: Applying the algorithm over a short time window ($w_l = 200$) identifies two clusters that exhibit transient periods of high ($\phi_c > 0.95$) and low synchrony. We label these 4 and 5 are use the same labels in all following tables and figures. a) The anatomical connectivity within and between each cluster. b) The instantaneous synchronization over time of each cluster (cluster membership identified by nodes of the same color). c) The instantaneous synchronization of the combination of both clusters.

T1-weighted and diffusion spectrum MRI. The density and length of fiber tracts were downsampled from an initial high-resolution scan covering 998 regions-of-interest (ROIs) and averaged over five subjects. The resulting network exhibits a densely connected and topologically and spatially central structural core, with a high degree of coupling between hemispheres (Figures 1 and 2a).

In [15] the same connectivity matrix is used to model BOLD fMRI resting-state activity. Each of the 66 anatomical regions in the matrix is replaced by a single Kuramoto oscillator, with connections between oscillators (weight matrix K and delay τ in Equation 1) derived from the average fiber density and length values produced in [4]. Within a given parameter regime the authors find that the model closely reproduces empirical observations of resting-state activity. In particular, the parameter space producing the closest match to empirical data results in dynamically complex behavior. Oscillators exhibit low global synchronization combined with the continuous and transient formation of highly synchronous subnetworks within model activity (Figure 2b). This is well-described by the dynamics of metastable chimera states seen in community-structured oscillator networks [20]. In Section III we present the results of applying hierarchical clustering on model output, using parameters from within the same region producing metastable behavior.

III. Results

The results of applying the clustering algorithm described in Section II-A to the output of the model of fMRI BOLD activity described in Section II-B are shown in Figures 3 and 4. The phase of each of the 66 oscillators in the model was recorded at each step of a simulation of 5 seconds of activity, with resolution r of 1.25 ms per time step. The natural frequency ω of each oscillator was set to $40Hz$ and the initial phase of each oscillator assigned randomly. The first 200 time steps of the simulation were discarded to allow for any initial network transient.

TABLE I: Correspondence between anatomical regions in the structural core [4] and highly-synchronous clusters (Figure 3). Regions in the structural core are listed by name and cluster membership indicated by the preceding number.

	left hemisphere	right hemisphere
posterior cingulate cortex	(1) lPC	(1) rPC
precuneus	(1) lPCUN	(1) rPCUN
cuneus	(1) lCUN	(1) rCUN
paracentral lobule	lPARC	(1) rPARC
isthmus of the cingulate	(1) lISTC	(1) rISTC
banks of the superior temporal sulcus	(2) lBSTS	(3) rBSTS
inferior parietal cortex	(2) lIP	(3) rIP
superior parietal cortex	(2) lSP	(3) rSP

We consider first the case of oscillators that remain highly synchronous ($\phi_c > 0.95$) over the entire simulation ($w_l = 4000$). We find three clusters within the model (Figure 3a) located in posterior and medial cortical regions that maintain a constant high level of internal synchronization (Figure 3b). Synchronous activity within posterior and right medial clusters

TABLE II: Correspondence between cortical "rich-club" regions [5] and synchronous clusters (Figures 3 and 4).

	left hemisphere	right hemisphere
superior frontal cortex	(4) lSF	(5) rSF
precuneus	(1) lPCUN	(1) rPCUN
paracentral lobule		(1) rPARC
superior parietal cortex	(2) lSP	(3) rSP
posterior cingulate cortex	(1) lPC	(1) rPC
isthmus of the cingulate	(1) lISTC	(1) rISTC
cuneus		(1) rCUN
lingual gyrus	(1) lLING	(1) rLING
pericalcarine cortex	(1) lPCAL	(1) rPCAL
caudal anterior cingulate cortex	lCAC	rCAC
rostral anterior cingulate cortex	(4) lRAC	
caudal middle frontal cortex		rCMF
entorhinal cortex	lENT	rENT
fusiform gyrus	lFUS	
parahippocampal cortex	lPARH	rPARH
superior temporal cortex	(2) lST	(3) rST

appears tightly coupled, while synchronization between these and the left medial cluster appears metastable (Figure 3c) displaying alternating periods of synchronization and desynchronization.

The correspondence of synchronous clusters to anatomical regions identified as falling within the structural core of the network is given in Table I. Each of the hub nodes forming the core of the network is contained in one of the highly-synchronous clusters with the exception of the left paracentral lobule (lPARC). The correspondence with cortical regions of a later "rich-club" analysis of connectivity data [5], a phenomenon where hub nodes within a network tend to be more densely connected with each other than with nodes of lower degree [21], is given in Table II. This study was based on more detailed connectivity data that included sub-cortical regions, we only include correspondence with regions present in the model. It is interesting that the left paracentral lobule is also absent from the "rich-club" network.

The result of searching for highly synchronous clusters ($\phi_c > 0.95$) over a shorter temporal window ($w_l = 200$, $w_s = 5$) is shown in Figure 4. In addition to the three synchronous clusters found previously, we identify two clusters (Figure 4a) occupying frontal cortical regions that display metastable synchronization dynamics (Figure 4b). The combined synchronization of both frontal clusters is shown in Figure 4c.

The authors of [4] also identify modular structure within the network through the application of spectral community detection [22]. The optimal partitioning of anatomical regions according to the connectivity matrix results in six modular regions. We find a strong correspondence between the modules identified within the network structure and clusters of synchronous activity in the model (Table III). The four frontal and medial clusters are a subset of each of four different modules, with the posterior cluster a subset of the remaining two modules. The spatial distribution of nodes within each cluster is given in Figure 5.

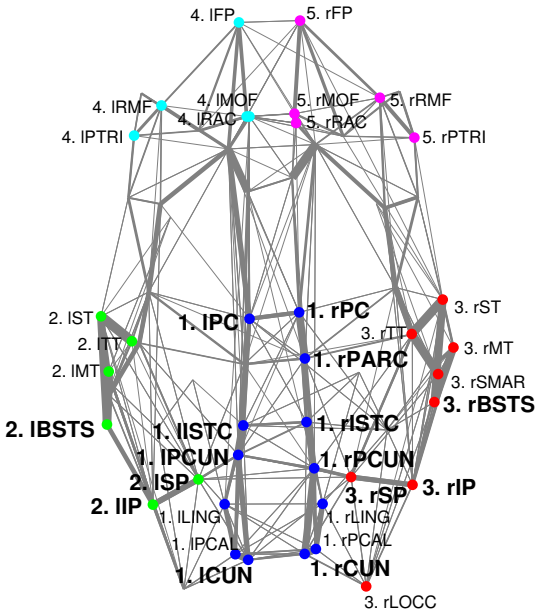

Fig. 5: Spatial representation of synchronous regions found through clustering. The spatial distribution of nodes within synchronous clusters shows a strong correspondence to modularity of the connectivity matrix, with each module containing oscillators from a single synchronous cluster.

IV. Conclusion

This paper presents a method for analyzing the temporal dynamics of synchronization between networks of coupled oscillators. The proposed algorithm applies hierarchical agglomerative clustering to the windowed time-series consisting of the phase of each interacting oscillator. The distance between clusters is based on a measure of instantaneous synchronization of all oscillators in the combined cluster. The method provides different views into cluster membership over time, and hence the dynamics of synchronization within the network, by varying the cut-off threshold for cluster membership and the window length and step size.

We demonstrate the relevance of the algorithm to the analysis of biological networks by applying it to an existing model of resting-state brain activity. The strong correspondence between synchronous clusters identified in model activity and the properties of the connectivity matrix on which the model is based is indicative of dynamical constraints placed on the activity within the network by underlying anatomical structure. Central hub nodes with a high degree of connectivity to other nodes in the network and to each other show significant overlap with nodes forming highly synchronous clusters. When we include clusters that display transient periods of high internal synchronization, we find an additional tendency for nodes in structural modules to synchronize with each other. There is much recent evidence of a functional role for synchronization in information transfer and integration between functionally segregated neural areas. It is interesting that synchronization

TABLE III: Correspondence between modular [4] and synchronous (Figures 3 and 4) clusters.

	left hemisphere		right hemisphere
Module 1	(1) lCUN		(1) rCUN
	(1) lLING		(1) rLING
	lPARH		
	(1) lPCAL		(1) rPCAL
	(1) lPCUN		
Module 2	lCAC		rCAC
	(1) lISTC		(1) rISTC
	lPARC		(1) rPARC
	(1) lPC		(1) rPC
			(1) rPCUN
Module 3	(2) lBSTS	Module 4	(3) rBSTS
	lENT		rENT
	lFUS		rFUS
	(2) lIP		(3) rIP
	lIT		rIT
	lLOCC		(3) rLOCC
	(2) lMT		(3) rMT
	lPSTC		rPSTC
	(2) lSP		(3) rSP
	(2) lST		(3) rST
	lSMAR		(3) rSMAR
	lTP		rTP
	(2) lTT		(3) rTT
			rPARH
Module 5	lCMF	Module 6	rCMF
	(4) lFP		(5) rFP
	lLOF		rLOF
	(4) lMOF		(5) rMOF
	lPOPE		rPOPE
	lPORB		rPORB
	(4) lTRI		(5) rTRI
	lPREC		rPREC
	(4) lRAC		(5) rRAC
	(4) lRMF		(5) rRMF
	(4) lSF		(5) rSF

of activity in the model appears related to both the degree and centrality of nodes and the distribution of spatially and topographically modular regions in network structure.

There are several avenues for further work. The method described in this paper would extend easily to other dynamical measures beyond the instantaneous synchronization of coupled oscillators. Considering the relative phase of synchronization between clusters may also produce interesting results for neural data, as would extending the method to include information theoretic measures such as transfer entropy [23] or causal density [24]. It would also be interesting to consider the response of the model to input simulating an external stimulus, and to apply the method to time-series data produced by modes of functional imaging such as EEG or fMRI. Finally, further investigation is required in the current model into the relationship between connectivity within and between structural modules and synchronization between nodes.

Acknowledgment

The authors acknowledge the support of Joana Cabral for providing and discussing the model of resting-state activity used in this paper.

References

[1] E. Bullmore and O. Sporns, "Complex brain networks: graph theoretical analysis of structural and functional systems," *Nature Reviews Neuroscience*, vol. 10, no. 3, pp. 186–198, 2009.

[2] D. S. Bassett and E. Bullmore, "Small-World brain networks," *Neuroscientist*, vol. 12, no. 6, pp. 512–523, 2006.

[3] D. J. Watts and S. H. Strogatz, "Collective dynamics of 'small-world' networks," *Nature*, vol. 393, no. 6684, pp. 440–442, 1998.

[4] P. Hagmann, L. Cammoun, X. Gigandet, R. Meuli, C. J. Honey, V. J. Wedeen, and O. Sporns, "Mapping the structural core of human cerebral cortex," *PLoS Biology*, vol. 6, no. 7, p. e159, 2008.

[5] M. P. van den Heuvel and O. Sporns, "Rich-Club organization of the human connectome," *The Journal of Neuroscience*, vol. 31, no. 44, pp. 15 775–15 786, 2011.

[6] R. Salvador, J. Suckling, M. R. Coleman, J. D. Pickard, D. Menon, and E. Bullmore, "Neurophysiological architecture of functional magnetic resonance images of human brain," *Cerebral Cortex*, vol. 15, no. 9, pp. 1332–1342, 2005.

[7] D. S. Bassett, A. Meyer-Lindenberg, S. Achard, T. Duke, and E. Bullmore, "Adaptive reconfiguration of fractal small-world human brain functional networks," *Proceedings of the National Academy of Sciences*, vol. 103, pp. 19 518–19 523, 2006.

[8] M. van den Heuvel, C. Stam, M. Boersma, and H. Hulshoff Pol, "Small-world and scale-free organization of voxel-based resting-state functional connectivity in the human brain," *NeuroImage*, vol. 43, no. 3, pp. 528–539, 2008.

[9] W. Liao, J. Ding, D. Marinazzo, Q. Xu, Z. Wang, C. Yuan, Z. Zhang, G. Lu, and H. Chen, "Small-world directed networks in the human brain: Multivariate granger causality analysis of resting-state fMRI," *NeuroImage*, vol. 54, no. 4, pp. 2683–2694, 2011.

[10] J. S. Damoiseaux and M. D. Greicius, "Greater than the sum of its parts: a review of studies combining structural connectivity and resting-state functional connectivity," *Brain Structure & Function*, vol. 213, no. 6, pp. 525–533, 2009.

[11] O. Sporns, "The human connectome: a complex network," *Annals of the New York Academy of Sciences*, vol. 1224, no. 1, pp. 109–125, 2011.

[12] C. J. Honey, J. Thivierge, and O. Sporns, "Can structure predict function in the human brain?" *NeuroImage*, vol. 52, no. 3, pp. 766–776, 2010.

[13] C. J. Honey, O. Sporns, L. Cammoun, X. Gigandet, J. P. Thiran, R. Meuli, and P. Hagmann, "Predicting human resting-state functional connectivity from structural connectivity," *Proceedings of the National Academy of Sciences*, vol. 106, no. 6, pp. 2035–2040, 2009.

[14] M. P. van den Heuvel, R. C. Mandl, R. S. Kahn, and H. E. H. Pol, "Functionally linked resting-state networks reflect the underlying structural connectivity architecture of the human brain," *Human Brain Mapping*, vol. 30, no. 10, pp. 3127–3141, 2009.

[15] J. Cabral, E. Hugues, O. Sporns, and G. Deco, "Role of local network oscillations in resting-state functional connectivity," *NeuroImage*, vol. 57, no. 1, pp. 130–139, 2011.

[16] G. Buzsaki and A. Draguhn, "Neuronal oscillations in cortical networks," *Science*, vol. 304, no. 5679, pp. 1926–1929, 2004.

[17] P. Fries, "Neuronal Gamma-Band synchronization as a fundamental process in cortical computation," *Annual Review of Neuroscience*, vol. 32, no. 1, pp. 209–224, 2009.

[18] R. Xu and D. Wunsch II, "Survey of clustering algorithms," *IEEE Transactions on Neural Networks*, vol. 16, no. 3, pp. 645–678, 2005.

[19] Y. Kuramoto, *Chemical oscillations, waves, and turbulence*. Springer, New York, 1984.

[20] M. Shanahan, "Metastable chimera states in community-structured oscillator networks," *Chaos*, vol. 20, no. 1, p. 013108, 2010.

[21] V. Colizza, A. Flammini, M. A. Serrano, and A. Vespignani, "Detecting rich-club ordering in complex networks," *Nature Physics*, vol. 2, no. 2, pp. 110–115, 2006.

[22] M. E. J. Newman, "Modularity and community structure in networks," *Proceedings of the National Academy of Sciences*, vol. 103, no. 23, pp. 8577–8582, 2006.

[23] T. Schreiber, "Measuring information transfer," *Physical Review Letters*, vol. 85, no. 2, pp. 461–464, 2000.

[24] A. K. Seth, A. B. Barrett, and L. Barnett, "Causal density and integrated information as measures of conscious level," *Philosophical Transactions of the Royal Society A*, vol. 369, no. 1952, pp. 3748–3767, 2011.